

Controlled Etching of Gold Nanorods Within Mesoporous Silica Shells at Mild Conditions

Kun-Peng Wang, Tian-Song Deng,* Er-Ji Zhang, Jia-Fei Gao, and Jie Liu

Surface plasmon resonance of precious metal gold nanorods can be tuned by controlling the aspect ratio, and they find widespread applications in biotechnology, imaging, sensing, optoelectronics, photonics, and catalysis. Here, a method is proposed for the controlled etching of gold nanorods within mesoporous silica shells by using a certain concentration of H_2O_2 at room temperature. In the experiments, the amount of HCl is varied to adjust the acidity and/or change the amount of H_2O_2 to control the speed of corrosion, achieving controllable adjustment of the aspect ratio of the gold nanorods. The extinction spectra show that under the action of H_2O_2 and HCl, the longitudinal plasmonic resonance of the gold nanorods shifted to shorter wavelengths, and the intensity of the longitudinal plasmonic resonance decreased. The more hydrochloric acid or hydrogen peroxide added, the faster the corrosion rate of the gold nanorods, and the faster the blue shift of the longitudinal plasmonic resonance. In addition, the intensity of the extinction spectra at 320 nm increased linearly versus time, which can also be used to monitor the etching process. By corroding gold nanorods to control the plasmonic resonances, gold nanorods can find broader applications.

1. Introduction

Gold nanorods (AuNRs) are a class of nanomaterials consisting of elemental gold in rod-like form. Typically, the size of AuNRs ranges from 80 to 130 nm in length and 10 to 50 nm in diameter, representing one-dimensional nanomaterials with aspect ratios ranging from 2 to 25. AuNRs exhibit two distinct surface plasmon resonances (SPRs), one associated with the longitudinal vibration mode of conduction electrons, and the other with the transverse vibration mode of conduction electrons. The transverse SPRs are in the visible spectrum, with a wavelength of $\approx 510\text{--}540$ nm, while the longitudinal SPRs can vary from visible light (≈ 600 nm) to the near-infrared range (>1200 nm).^[1–4] AuNRs not only demonstrate anisotropic optical properties dependent on aspect ratio but also feature excellent biocompatibility, ease of fabrication, and the ability to bind with various biomolecular ligands,

antibodies, and other targeting moieties, rendering them hot subjects in nanomaterial research. Currently, AuNRs find favorable applications in biochemical sensing, biomedical imaging, and medical diagnostics.^[5–9]

The diameter of AuNRs serves as a significant distinguishing factor in their applications. For instance, the extinction is primarily determined by the absorption of thin AuNRs (diameter <15 nm), making them highly suitable for photothermal applications requiring high photon-thermal conversion efficiency.^[7] In contrast, thicker AuNRs (diameter >30 nm) are dominated by scattering, making them advantageous for applications such as bioimaging and optical signal enhancement, including metal-enhanced fluorescence and surface-enhanced spectroscopy.^[10] For AuNRs, their sizes predominantly imply their aspect ratio, making the aspect ratio highly important. AuNRs are typically synthesized via seed-mediated growth, with a yield of

over 97% and a relative size deviation of $<10\%$. Seed-mediated growth involves the influence of stabilizing surfactant hexadecyl trimethyl ammonium bromide (CTAB) and shape-inducing agent Ag^+ , as well as the adjustment of the acidity of the growth solution, to roughly control the aspect ratio of AuNRs. The use of silver ion-assisted seed-mediated methods for preparing initial AuNRs, coupled with a CTAB-NaOL binary surfactant mixture, significantly extended the size tunability of AuNRs achievable through a one-pot seed-mediated growth process.^[11–14] However, the seed growth method for synthesis under higher concentrations of CTAB is restricted due to the toxicity of CTAB, limiting its biomedical applications. Therefore, related studies have confirmed that selective etching after the growth of AuNRs can also more precisely control the aspect ratio of AuNRs.

The etching methods have been successfully demonstrated through $\text{Fe}^{3+}/\text{Cu}^{2+}/\text{H}_2\text{O}_2$,^[15] $\text{Br}^-/\text{H}_2\text{O}_2$,^[16,17] $\text{SCN}^-/\text{H}_2\text{O}_2$,^[18–21] e-beam,^[22] Au^{3+} ,^[23,24] O_2 ,^[25] and H_2O_2 .^[26–28] Etching primarily occurs at the ends of the nanorods, maintaining a constant diameter.^[15,17,21,26] Consequently, the nanorods are selectively shortened, achieving more precise control over the aspect ratio.^[29] Initially, these etching processes were carried out in AuNRs solutions containing high concentrations of CTAB.^[30] However, the toxicity of CTAB poses issues when using AuNRs for in vivo studies. Additionally, in catalytic applications, the dense surfactant layer hinders the interaction

K.-P. Wang, T.-S. Deng, E.-J. Zhang, J.-F. Gao, J. Liu
 School of Electronics and Information Engineering
 Hangzhou Dianzi University
 Hangzhou 310018, P. R. China
 E-mail: dengts@pku.edu.cn

The ORCID identification number(s) for the author(s) of this article can be found under <https://doi.org/10.1002/ppsc.202400144>

DOI: 10.1002/ppsc.202400144

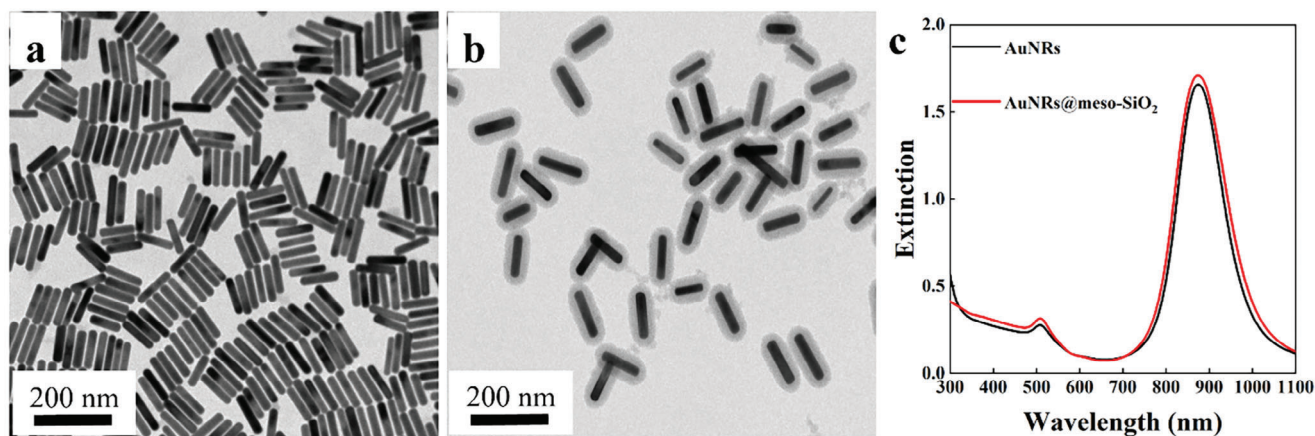


Figure 2. a) TEM image of AuNRs; b) TEM image of AuNRs@meso-SiO₂; (c) UV-vis-NIR absorption spectra of AuNRs (black curve) and AuNRs@meso-SiO₂ (red curve).

Figure 3a shows the color changes of the solution at intervals of 5 minutes, from the start (0 min) to the end (30 min) of the corrosion reaction. It is evident that as the corrosion reaction progresses, the color transitions from brownish to ultimately transparent. These changes correspond directly with the spectral data presented in **Figure 3b**. As depicted in **Figure 3b**, the spectra illustrate that under acidic conditions, hydrogen peroxide facilitates the rapid oxidation and corrosion of the gold nanorods, resulting in a blue shift in the longitudinal resonance peak and a noticeable decrease in its intensity. Meanwhile, the position of

the transverse resonance peak of the gold nanorods remains relatively unchanged, with only intensity variations occurring. The curves in **Figure 3c,d** respectively depict the trends in the changes of the longitudinal resonance peak and its intensity, both showing a linear trend. According to the empirical formula:

$$\lambda_{\max} = 95R + 450 \quad (1)$$

where λ_{\max} represents the longitudinal resonance peak of the gold nanorods, and R denotes the aspect ratio (length-to-width)

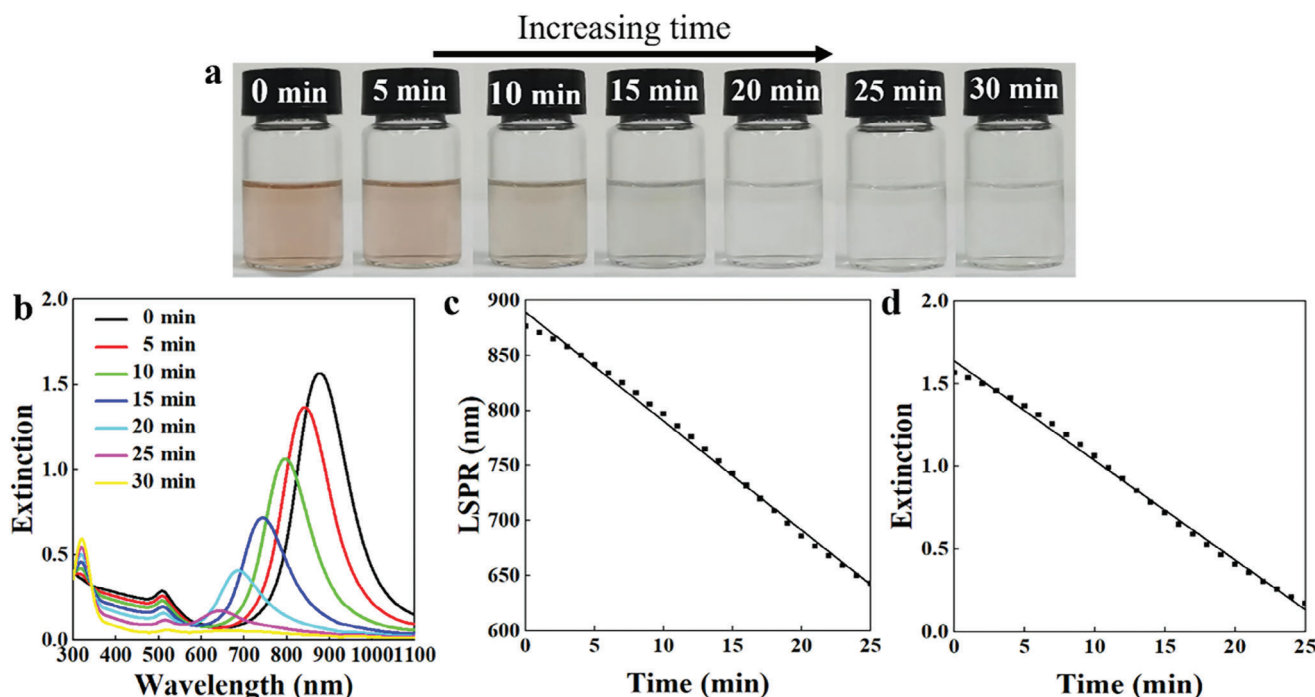


Figure 3. a) Real-time images showing the corrosion of gold nanorods in a 1 mL methanol solution with 60 μ L hydrochloric acid (37 wt.% in water) and 50 μ L hydrogen peroxide (30 wt.% in H₂O, diluted 25 times in methanol solution), b) spectral graphs illustrating the evolution of the corrosion of gold nanorods over time, c) Changes in the longitudinal resonance peak position of the gold nanorods over time, d) Variation in the intensity at LSPR of the gold nanorods over time.

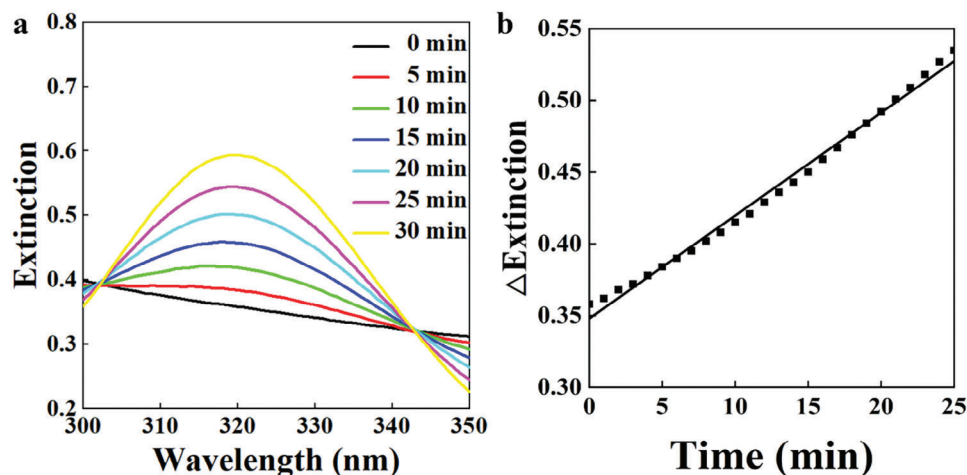


Figure 4. a) The spectral graph of gold nanorods within the wavelength range of 300 to 350 nm; b) The change of the intensity at 320 nm of gold nanorods over time.

ratio) of the gold nanorods. Verification reveals that λ_{\max} is ≈ 830 to 906 nm, which falls within an acceptable range of error. The longitudinal resonance peak measured by the spectrophotometer for the prepared nanorods aligns with the value obtained from the empirical formula. The slope of the fitted line from Figure 3c revealed the blueshift of LSPR was 9.0 nm min^{-1} , and the decrease of extinction intensity was -0.061 min^{-1} (Figure 3d).

Figure 4a shows the spectral graph of gold nanorods in the wavelength range of 300 to 350 nm. By observing the spectrum from 300 to 350 nm, a significant peak is observed at around 320 nm, with its intensity gradually increasing, while the intensity around 342 nm remains relatively constant. The increase in intensity at 320 nm is attributed to the oxidation of Au^0 to Au^{3+} ions, which form AuCl_4^- ions (due to the addition of HCl), exhibiting spectral characteristics at 320 nm. By observing the intensity change at 320 nm (the slope is 0.0075 min^{-1}) during corrosion, the process of the etching could be monitored.

From Figure 5a, it can be observed that the prepared gold nanorods within mesoporous SiO_2 shells are relatively uniformly distributed, with minimal variation in size among individual nanorods. Figure 5b–e demonstrated that the nanorods within the mesoporous silica started to corrode from both ends, with the diameter of the gold nanorods remaining nearly unchanged while the length gradually decreased, resulting in a reduction in the aspect ratio of the gold nanorods. As corrosion proceeded, the gold nanorods were eventually completely corroded. In Figure 5f, only the empty SiO_2 shell remained, indicating complete corrosion of the gold nanorods. As the length-to-width aspect ratio of the gold nanorods decreases, a significant change in the corresponding color of the gold nanorods solution could also be observed. As shown in the insets of Figure 5, the color gradually became lighter, and finally transparent.

AuNRs have a face-centered cubic (FCC) crystal structure, with a lattice constant of $\approx 4.08 \text{ \AA}$. Figure 6a shows a high-resolution

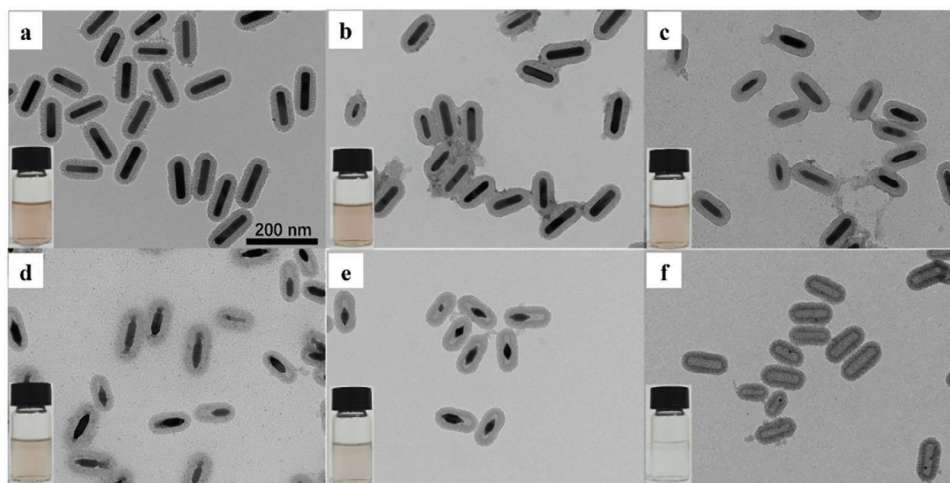


Figure 5. Transmission electron microscopy images of AuNRs@meso- SiO_2 at different stages of corrosion and the changes of gold nanorods in the bottle. a) Initial gold nanorods (0 min); b–e) Different stages of gold nanorod corrosion: (b) 5 min, (c) 10 min, (d) 15 min, (e) 20 min; f) complete corrosion of gold nanorods (30 min).

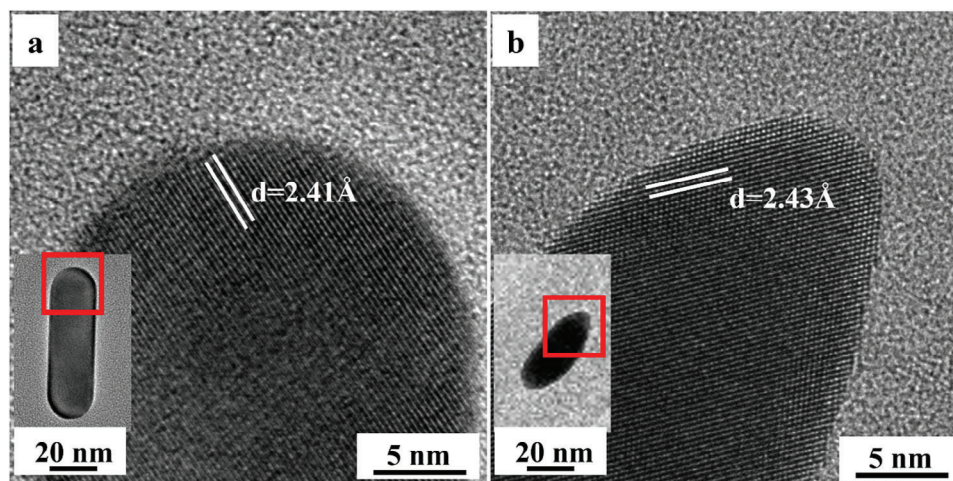
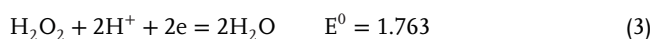
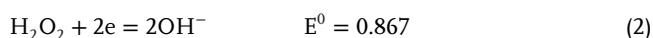


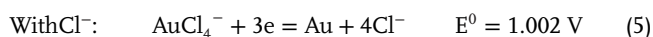
Figure 6. a) HRTEM image of the initial gold nanorod (0 min); b) HRTEM image of the gold nanorod corrosion (20 min). The inset at the lower left corner shows a single gold nanorod, where the red square area indicates the HRTEM imaging area.

TEM (HRTEM) image of the initial, unetched gold nanorod, with a measured crystal plane spacing of 2.41 Å, corresponding to the (111) plane of Au. Figure 6b shows an HRTEM image of the gold nanorod after 20 min of etching. It is evident that the tips of the nanorods have been significantly etched, becoming sharper, while their width remains largely unchanged. This observation is consistent with the experimental findings mentioned above. Additionally, the crystal plane spacing of the etched gold nanorod is 2.43 Å, which also corresponds to the (111) plane of Au. Therefore, it can be concluded that the etching of the gold nanorods begins along the (111) crystal planes. This HRTEM imaging provides a clearer understanding of the etching behavior of the gold nanorods.

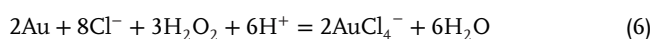
According to the standard reduction potentials (vs the normal hydrogen electrode (NHE)) of the related half reactions^[39]



Au(0)/Au(III) reaction



We propose the following overall reaction for the oxidative etching process:



Here, H^+ enhances the reduction potential of the H_2O_2 half-reaction from 0.867 to 1.763 V (vs NHE), while Cl^- acts as a complexing agent, which reduces the reduction potential of Au(0)/Au(III) from 1.52 to 1.002 V (vs NHE).

1.3. The Performance under Different Hydrochloric Acid Conditions

The amounts of hydrogen peroxide and hydrochloric acid have a significant impact on the corrosion process of gold nanorods. We initially investigated the effect of varying the amount of hydrochloric acid on the corrosion process. The same amount of hydrogen peroxide (50 μL , 30 wt % in water, diluted 25 times in methanol solution) was added to the AuNRs@meso- SiO_2 solution, followed by the addition of 80, 60, 40, and 0 μL of hydrochloric acid (37 wt.% in water), respectively. The changes in the extinction spectra of gold nanorods with the addition of different amounts of hydrochloric acid, while keeping the amount of hydrogen peroxide constant, were compared. These changes were plotted as curves and linear fitting was performed.

From Figure 7a, the blueshift rates of LSPR are 11.6 nm min^{-1} (80 μL), 9.0 nm min^{-1} (60 μL), 6.3 nm min^{-1} (40 μL), and 0 nm min^{-1} (0 μL), respectively. From Figure 7b, the decrease rates of LSPR intensity after adding 80, 60, 40, and 0 μL of hydrochloric acid are -0.077 , -0.061 , -0.045 , and 0 min^{-1} , respectively. According to Figure 7c, the slopes of the fitted lines (intensity change at 320 nm) after adding 80, 60, 40, and 0 μL of hydrochloric acid are 0.0098, 0.0075, 0.0054, and 0 min^{-1} , respectively. It can be concluded that when no hydrochloric acid is added, the gold nanorods are not corroded, which is consistent with the theoretical analysis based on the standard reduction potentials of the related half-reactions. However, when hydrochloric acid is added, the gold nanorods begin to corrode, and with increasing amounts of hydrochloric acid, the corrosion rate at both ends of the gold nanorods increases, leading to a faster blueshift of the longitudinal resonance peak, a quicker decrease in spectral intensity, and a more rapid change in the intensity difference at 320 nm. We chose 80 μL of hydrochloric acid as the upper limit for the control group because we found that adding higher concentrations of hydrochloric acid causes the corrosion rate to be too rapid, shortening the overall reaction time and making it difficult to achieve gold nanorods with the desired length-to-diameter ratio in a controlled manner.

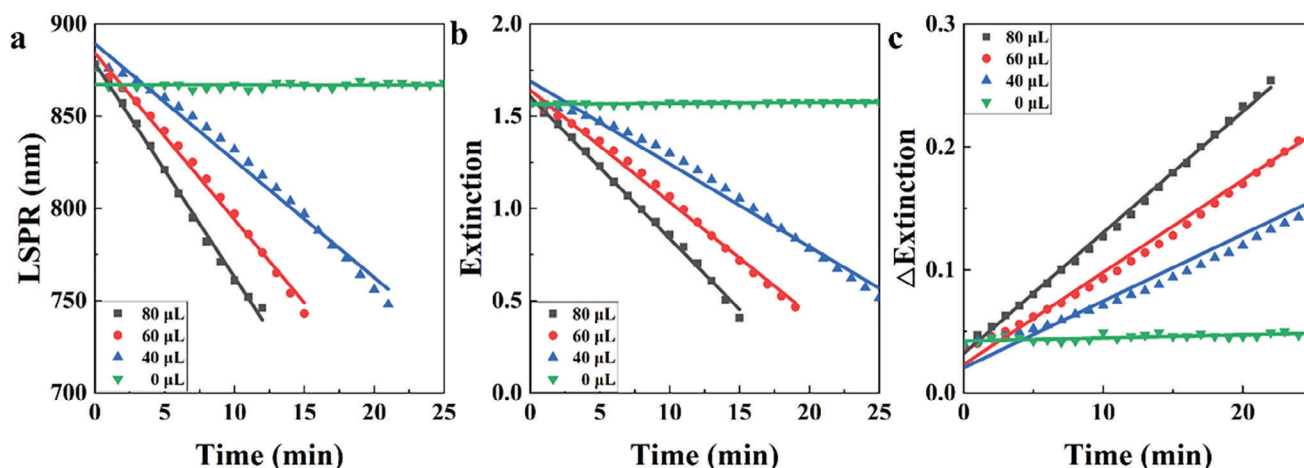


Figure 7. Variation of the longitudinal resonance peak position a), intensity of LSPR b), and intensity at 320 nm c) over time with the addition of 80, 40, and 0 μL hydrochloric acid (37 wt.% in water).

1.4. The Performance under Varying Amounts of Hydrogen Peroxide

Next, we explored the influence on the corrosion process by varying the amount of hydrogen peroxide. The same amount of hydrochloric acid (60 μL, 37 wt.% in water) was added to the AuNRs@meso-SiO₂ solution, followed by the addition of 70, 50, and 30 μL of hydrogen peroxide (30 wt.% in water, diluted 25 times in methanol solution), respectively. The changes in the absorption spectra of gold nanorods with different amounts of hydrogen peroxide, while keeping the amount of hydrochloric acid constant, were compared. These changes were plotted as curves and linear fitting was performed to obtain straight lines, except for the experiment with 30 μL of hydrogen peroxide where significant curve changes prevented line fitting.

From Figure 8a, the blueshift of LSPR were $-14.0 \text{ nm min}^{-1}$ (70 μL) and -9.0 nm min^{-1} (50 μL), respectively. From Figure 8b, the decrease of LSPR intensity for the addition of 70 and 50 μL of hydrogen peroxide was -0.093 and -0.061 min^{-1} , respectively.

From Figure 8c, the slopes of the fitted lines (the intensity change at 320 nm) for the addition of 70 and 50 μL of hydrogen peroxide were 0.012 and 0.0075 min^{-1} . Although the experiment with 30 μL of hydrogen peroxide did not fit into a straight line, it still shows slower curve changes.

It can be concluded that when the amount of hydrochloric acid is kept constant, a higher amount of hydrogen peroxide leads to a faster corrosion rate at both ends of the gold nanorods, resulting in a quicker blue shift of the longitudinal resonance peak, a faster decrease in spectral intensity, and a quicker change in the intensity difference 320 nm.

In comparison with the experimental data of Wen T^[15] and Weng G^[16] on the oxidation of AuNRs, they were corroding gold nanorods using Fe³⁺/Cu²⁺/H₂O₂ and Br⁻/H₂O₂ respectively. It was observed that none of them exhibited excellent linear relationships over time. Conversely, our experimental results demonstrated a strong linear correlation with time. In comparison with the experimental data of Wu Z^[23] on the oxidation of AuNRs, they corroded gold nanorods using Au(III), our experimental costs are

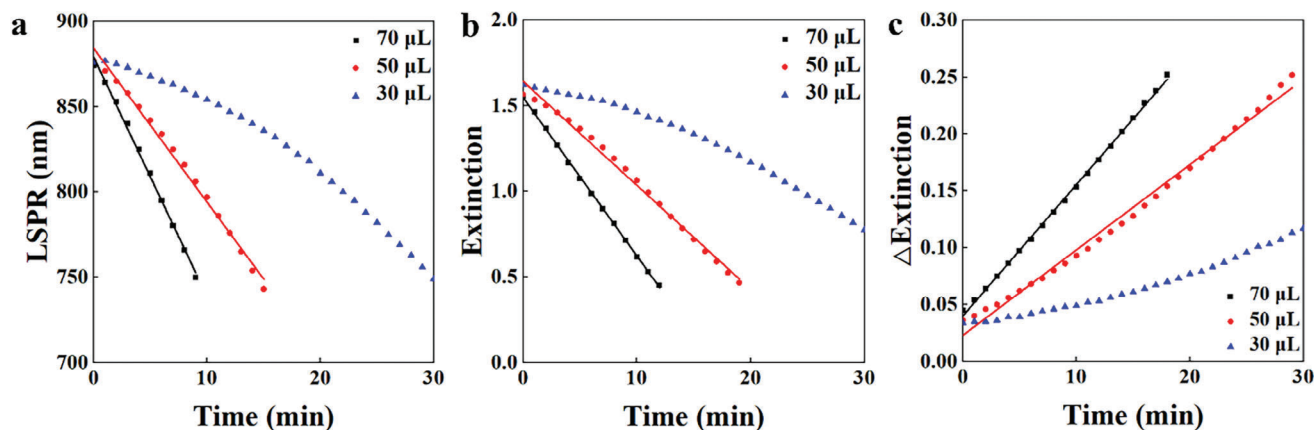


Figure 8. Variation of the longitudinal resonance peak position a), intensity of LSPR b), and intensity at 320 nm c) over time with the addition of 70, 50, and 30 μL of hydrogen peroxide (30 wt.% in water, diluted 25 times in methanol solution).

much cheaper. In comparison to Yuan HF's^[27] experiments on etching gold nanorods, where the LSPR transfer rate was 110 nm h⁻¹ during the first two hours and then decreased to 26 nm h⁻¹ over the following four hours, our etching process has a rate of 40 nm min⁻¹. Not only is our rate faster, but it also remains constant throughout the entire etching process. In comparison with the experimental data of Wang JF^[30] on the oxidation of AuNRs, she corroded gold nanorods with H₂O₂ under high CTAB (0.1 M) concentration conditions, while our experiment for etching gold nanorods does not require the addition of CTAB, which is beneficial for the application of the samples in in vivo detection.

2. Conclusion

Gold nanorods were prepared using the seed-mediated growth method, followed by encapsulation with mesoporous silica. Subsequently, controlled etching of the gold nanorods was achieved by adding a certain amount of hydrogen peroxide and hydrochloric acid at room temperature, enabling adjustment of the aspect ratio and longitudinal resonance absorption peak position. The corrosion behavior of the gold nanorods was investigated under different reaction times, concentrations of hydrogen peroxide, and concentrations of hydrochloric acid. Experimental results demonstrated that, under the influence of hydrogen peroxide and hydrochloric acid, the gold nanorods underwent corrosion, resulting in a blue shift of the longitudinal resonance absorption peak, a decrease in its intensity, and a significant intensity change at 320 nm, which exhibited a linear relationship with time. Electron microscopy images revealed that the corrosion of the gold nanorods initiated from both ends, with minimal change in diameter. This method allows for significant adjustment of the longitudinal resonance absorption peak position of gold nanorods at room temperature, offering broader potential applications in medical imaging,^[5,17,40] cell detection,^[9,29] photocatalysis,^[34] and SERS.^[8,33,35,37]

3. Experimental Section

Materials: All chemicals were purchased and used without further purification. Hexadecyltrimethylammonium bromide (CTAB, >98.0%), sodium oleate (NaOL, >97.0%), Chloroauric acid (HAuCl₄), sodium hydroxide (98%), L-ascorbic acid (AA, ≥99.5%), silver nitrate (AgNO₃, ≥99%), sodium borohydride (NaBH₄, 99%), hydrochloric acid (HCl, 37.0 wt.% in water), tetraethyl orthosilicate (TEOS, 98%), hydrogen peroxide (H₂O₂, 30 wt.% in water), and methanol (MeOH, ≥99.99%) were used. Ultrapure water (Millipore Milli-Q grade) with a resistivity of 18.2 MΩ was used in all of the experiments. All glassware for AuNRs synthesis was cleaned with fresh aqua regia (HCl/HNO₃ in a 3:1 ratio by volume; caution! Aqua regia is extremely corrosive and should be handled with extreme care!) and rinsed with large amounts of water.

Preparation of Gold Nanorods: Gold nanorods (AuNRs) were synthesized using an improved seed-mediated method.^[12] A seed solution was prepared by adding HAuCl₄ (0.05 M, 50.0 μL) to CTAB (0.1 M, 10.0 mL) in a 20 mL scintillation vial. Then, freshly prepared ice-cold NaBH₄ solution (0.01 M, 0.60 mL) was rapidly injected into the Au(III)-CTAB solution with vigorous stirring (1200 rpm) for 2 min. The seed solution was kept at 30 °C for at least 30 minutes before use. To grow the AuNRs, CTAB (7.0 g) and NaOL (1.234 g) were dissolved in warm water (≈50 °C, 250 mL) until completely dissolved. The solution was then cooled to 30 °C, and AgNO₃ solution (0.01 M, 7.2 mL) was added. After 15 min of standing, HAuCl₄ solution (1 mM, 250 mL) was added. The solution was stirred for 90 min

(400 rpm), followed by the addition of HCl (37 wt.% in water, 2.1 mL) and stirring (400 rpm) for 15 min. Subsequently, L-ascorbic acid solution (0.064 M, 1.25 mL) was added, and the solution was vigorously stirred for 30 s. Finally, the seed solution (0.80 mL) was injected into the growth solution. The solution was stirred for 1 min and allowed to stand at 30 °C for 12 hours for AuNRs growth. The extinction spectrum of the gold nanorods was measured, and those with higher intensity and better spectral curves were selected for subsequent experiments involving coating with mesoporous silica and etching, as observed under electron microscopy.

Coating with Mesoporous Silica: Prior to coating with mesoporous SiO₂,^[41] the synthesized AuNRs solution (20 mL) was centrifuged at 6000 rpm for 30 min and the supernatant was removed. The obtained precipitate was then redispersed in water until homogeneous and centrifuged again to remove the supernatant. The precipitate was then redispersed in a CTAB solution (6 mL, 1.5 mM). While stirring at 400 rpm, NaOH solution (0.1 M, 0.06 mL) was added, and TEOS solution (20 v% in methanol, 0.018 mL) was added every 60 min, three times in total. The reaction was allowed to continue for 2 days with stirring to form a mesoporous SiO₂ shell with a thickness of ≈18 nm. The resulting particles were washed with water and methanol solutions, and the particles were dispersed in methanol (30 mL) for subsequent etching experiments.

Etching of Gold Nanorods: A novel method was employed here, where a certain concentration of hydrogen peroxide was used for oxidation etching of monodisperse gold nanorods within the mesoporous silica shell at room temperature, allowing precise control over the aspect ratio. The oxidation rate can be altered by varying the concentration of acid and/or temperature. In a glass bottle, the AuNRs@meso-SiO₂ solution (1.0 mL in methanol) was mixed with 60 μL of HCl (37 wt.% in water) and 50 μL of H₂O₂ (diluted 25 times, 30wt.% in H₂O). The bottle was sealed to prevent solution evaporation. As the etching time increased, the color of the solution changed, observed by taking a photo of the object every minute. The etching rate was controlled by adjusting the amount of HCl (80, 60, 40, and 0 μL) or H₂O₂ (70, 50, and 30 μL). The oxidation process was monitored by measuring the extinction spectrum.

Characterizations: Optical extinction spectra were recorded with a UV-1900i spectrophotometer (SHIMADZU, Japan) with a 1.0 cm optical path. The transmission electron microscope (TEM) images were obtained with an HT-7700 microscope (HITACHI, Japan) operated at 100 kV. HRTEM images were performed using a JEM-F200 TEM (JEOL, Japan) with a 200 kV acceleration voltage. The particle sizes of the nanoparticles were measured from TEM images using ImageJ software, with measurements taken from more than 100 nanoparticles for each sample.

Acknowledgements

The authors thank Sudan Shen for her assistance in TEM at the State Key Laboratory of Chemical Engineering (Zhejiang University). T.S.D. acknowledges financial support from Zhejiang Provincial Natural Science Foundation (Grant: LY24F050008), Zhejiang Provincial Educational Ministry Scientific Research Project (Grant: Y202352284), and National Natural Science Foundation of China (NSFC, Grant: 61905056). This work was also supported by the Fundamental Research Funds for the Provincial Universities of Zhejiang (GK239909299001-301).

Conflict of Interest

The authors declare no conflict of interest.

Data Availability Statement

The data that support the findings of this study are available from the corresponding author upon reasonable request.

Keywords

corrosion, gold nanorods, mesoporous silica shells, seed growth method, surface plasmon resonance

Received: June 24, 2024
Revised: August 6, 2024
Published online:

- [1] R. Sardar, A. M. Funston, P. Mulvaney, R. W. Murray, *Langmuir* **2009**, 25, 13840.
- [2] N. J. Halas, S. Lal, W.-S. Chang, S. Link, P. Nordlander, *Chem. Rev.* **2011**, 111, 3913.
- [3] H. Chen, L. Shao, Q. Li, J. Wang, *Chem. Soc. Rev.* **2013**, 42, 2679.
- [4] J. P. Zheng, X. Z. Cheng, H. Zhang, X. P. Bai, R. Q. Ai, L. Shao, J. F. Wang, *Chem. Rev.* **2021**, 121, 13342.
- [5] L. Vigderman, B. P. Khanal, E. R. Zubarev, *Adv. Mater.* **2012**, 24, 4811.
- [6] B. D. Chithrani, A. A. Ghazani, W. C. W. Chan, *Nano Lett.* **2006**, 6, 662.
- [7] X. H. Huang, I. H. El-Sayed, W. Qian, M. A. El-Sayed, *J. Am. Chem. Soc.* **2006**, 128, 2115.
- [8] P. K. Jain, X. Huang, I. H. El-Sayed, M. A. El-Sayed, *Acc. Chem. Res.* **2008**, 41, 1578.
- [9] P. K. Jain, K. S. Lee, I. H. El-Sayed, M. A. El-Sayed, *J. Phys. Chem. B* **2006**, 110, 7238.
- [10] R. Thomas, J. Kumar, R. S. Swathi, K. G. Thomas, *Curr. Sci.* **2012**, 102, 85.
- [11] N. Abid, M. Khan, S. Shujait, K. Chaudhary, M. Ikram, M. Imran, J. Haider, M. Khan, Q. Khan, M. Maqbool, *Adv. Colloid Interface Sci.* **2022**, 300, 102597.
- [12] X. C. Ye, C. Zheng, J. Chen, Y. Z. Gao, C. B. Murray, *Nano Lett.* **2013**, 13, 765.
- [13] B. Nikoobakht, M. A. El-Sayed, *Chem. Mater.* **2003**, 15, 1957.
- [14] F. Kim, J. H. Song, P. Yang, *J. Am. Chem. Soc.* **2002**, 124, 14316.
- [15] T. Wen, H. Zhang, X. Tang, W. Chu, W. Liu, Y. Ji, Z. Hu, S. Hou, X. Hu, X. Wu, *J. Phys. Chem. C* **2013**, 117, 25769.
- [16] G. Weng, X. Dong, J. Li, J. Zhao, *J. Mater. Chem. C* **2016**, 51, 7678.
- [17] L. Saa, M. Coronado-Puchau, V. Pavlov, L. M. Liz-Marzán, *Nanoscale* **2014**, 6, 7405.
- [18] S. Lu, L. Chen, P. Yang, K. Matras-Postolek, *RSC Adv.* **2016**, 6, 19620.
- [19] S. Lee, Y.-S. Nam, S.-H. Choi, Y. Lee, K.-B. Lee, *Microchim. Acta* **2016**, 183, 3035.
- [20] P. Free, G. Conger, S. J. Wu, J. B. Zhang, D. G. Fernig, *Colloid Surf. B-Biointerfaces* **2016**, 146, 871.
- [21] Z. Zhang, Z. Chen, D. Pan, L. Chen, *Langmuir* **2014**, 31, 643.
- [22] W. Wang, T. Xu, T. T. Bai, C. Zhu, Q. B. Zhang, H. T. Zhang, H. Zhang, Z. R. Guo, H. M. Zheng, L. T. Sun, *Sci. China-Mater.* **2020**, 63, 2599.
- [23] Z. Wu, Y. Liang, Q. Guo, K. Zhang, S. Liang, L. Yang, Q. Xiao, D. Wang, *J. Mater. Chem. C* **2019**, 54, 8133.
- [24] J. Rodríguez-Fernández, J. Pérez-Juste, P. Mulvaney, L. M. Liz-Marzán, *J. Phys. Chem. B* **2005**, 109, 14257.
- [25] C. K. Tsung, X. S. Kou, Q. H. Shi, J. P. Zhang, M. H. Yeung, J. F. Wang, G. D. Stucky, *J. Am. Chem. Soc.* **2006**, 128, 5352.
- [26] L. Saa, R. Grinyte, A. Sánchez-Iglesias, L. M. Liz-Marzán, V. Pavlov, *ACS Appl. Mater. Interfaces* **2016**, 8, 11139.
- [27] H. F. Yuan, K. P. F. Janssen, T. Franklin, G. Lu, L. Su, X. Gu, H. Uji-i, M. B. J. Roeflaers, J. Hofkens, *RSC Adv.* **2015**, 5, 6829.
- [28] G. Chandrasekar, K. Mougín, H. Haidara, L. Vidal, E. Gnecco, *Appl. Surf. Sci.* **2011**, 257, 4175.
- [29] K. Kermanshahian, A. Yadegar, H. Ghourchian, *Coord. Chem. Rev.* **2021**, 442, 213934.
- [30] W. H. Ni, X. Kou, Z. Yang, J. F. Wang, *ACS. Nano* **2008**, 2, 677.
- [31] I. Gorelikov, N. Matsuura, *Nano Lett.* **2008**, 8, 369.
- [32] H. Yu, R. X. Zheng, F. Lei, W. Y. Wang, W. K. Guo, L. Zhang, Y. D. Liu, X. W. Chen, Y. X. Wang, *Am. J. Transl. Res.* **2022**, 14, 1518.
- [33] Y. Zhang, J. Qian, D. Wang, Y. Wang, S. He, *Angew. Chem.-Int. Edit.* **2013**, 52, 1148.
- [34] A. Sakthisabarimoorathi, S. Dhas, M. Jose, *Mater. Chem. Phys.* **2020**, 240, 122154.
- [35] L. Xu, A. H. Yao, T. Zhou, D. P. Wang, *Rare Metal Mater. Eng.* **2016**, 45, 1066.
- [36] E. Cepeda-Pérez, T. López-Luke, P. Salas, G. Plascencia-Villa, A. Ponce, J. Vivero-Escoto, M. José-Yacaman, E. de la Rosa, *Biomed. Opt. Express* **2016**, 7, 2407.
- [37] D. Fernand, C. Pardanaud, D. Bergé-Lefranc, P. Gallice, V. Hornebecq, *J. Phys. Chem. C* **2014**, 118, 15308.
- [38] T.-S. Deng, J. E. S. van der Hoeven, A. O. Yalcin, H. W. Zandbergen, M. A. van Huis, A. van Blaaderen, *Chem. Mater.* **2015**, 27, 7196.
- [39] R. Long, S. Zhou, B. J. Wiley, Y. Xiong, *Chem. Soc. Rev.* **2014**, 43, 6288.
- [40] X. Fu, J. Cai, X. Zhang, W.-D. Li, H. Ge, Y. Hu, *Adv. Drug Delivery Rev.* **2018**, 132, 169.
- [41] Z. Wu, Q. Zeng, H. Wang, *J. Mater. Chem. C* **2016**, 4, 2614.